Unified model for Mullins effect and high cycle fatigue life prediction of rubber materials

Laurent Gornet, Gilles Marckmann, R. Desmorat, Pierre Charrier

Unified model for Mullins effect and high cycle fatigue life prediction of rubber materials

L. Gornet & G. Marckmann
GeM, UMR CNRS 6183, Ecole Centrale Nantes, 1 rue de la Noë, BP 92101-44321 Nantes, Cedex 3, France.

R. Desmorat
LMT- Cachan ENS Cachan/CNRS/UPMC/PRES UniverSud Paris, 61 avenue du Président Wilson, F-94230 Cachan Cedex, France.

P. Charrier
TrelleborgVibracoustic, Zone ind. de Carquefou, BP 419, 44474 Carquefou Cedex – France

ABSTRACT: The study describes the basic principles of a general damage model (GDMF) for Mullins effect and high cycle fatigue loadings of rubber materials and demonstrates its prediction possibilities for simulating the complete fatigue failure phenomenon. The present paper focuses on stiffness modelling of rubber materials for uniaxial and multiaxial static and fatigue loadings with a minimal number of material parameters in order to ensure robustness of the identification. The proposed hyperplastic model is expressed in terms of classical independent strain invariants. Mullins effect and high cycle fatigue loadings are both modelled according to a continuum damage mechanics approach.

1 INTRODUCTION

The aim of the present paper is to develop new constitutive model for lifetime prediction of elastomers which are physically motivated, well adapted for numerical problems, and accurate for rubber materials under multiaxial high cycle fatigue loadings. We propose a strain energy function expressed in terms of independent strain invariants restricted, in the present paper, to uniaxial high cyclic loadings. A way to predict the fatigue life is to calculate the damage accumulation cycle by cycle using the continuum damage mechanics approach (Lemaitre & Chaboche 1990). For rubber-like materials, CDM approaches are mainly focused on the Mullins effect (Chagnon et al. 2004, 2006, Cantournet 2002, Cantournet et al. 2009). Few models are developed for fatigue phenomena (Wang et al. 2002, Ayoub et al. 2012). In the present study, the damage model (Gornet et al. 2012) initially developed for the multiaxial Mullins effect (few cycles) is extended to high cycle fatigue loadings. In the Finite Element context, the proposed model can easily be implemented thanks to its strain invariants formulation. Finite Element predictions of samples have been carried out with the Finite Element code Abaqus.

2 STRAIN ENERGY FUNCTION

In this section, the hyperelastic strain energy function that defines the foundation of the proposed fatigue model is briefly recalled. For incompressible materials, a phenomenological energy function is expressed in term of the first I_1 and the second invariant I_2 (Gornet *et al.* 2012).

2.1 *Incompressible GD strain energy density*

Assuming that rubber materials are both isotropic and incompressible, the proposed strain energy function W only depends on the two first invariants of the left Cauchy-Green stretch tensor B:

$$\begin{aligned} W_{GD}\left(I_1,I_2\right) &= W_1\left(I_1\right)+W_2\left(I_2\right) \\ &= h_1\int e^{h_3(I_1-3)^2}dI_1 + 3h_2\int\frac{1}{\sqrt{I_2}}dI_2 \end{aligned} \tag{1}$$

where h_1, h_2, h_3 are the material parameters. In this strain energy, the term depending on I_1 of W describes the global response of the material and is similar to the first part of the Hart-Smith model (Hart-Smith 1966). The second term that involves I_2 improves the accuracy of the model for multiaxial loading conditions (a general power I_2-term has been introduced by Lambert-Diani & Rey, 1999). The true stress tensor is defined by the differentiation of the proposed strain energy with respect to B:

$$\sigma = -pI + 2\left(\frac{\partial W}{\partial I_1}+I_1\frac{\partial W}{\partial I_2}\right)B - 2\frac{\partial W}{\partial I_2}B^2 \tag{2}$$

$$I_1 = Tr(B),\ I_2 = \frac{1}{2}\left[Tr(B)^2 - Tr(B^2)\right] \quad (3)$$

2.2 *Links between GD and eight-chains models*

The hyperelastic model is characterized by its ability to describe the strain-hardening of the material that takes place under large strains. This strain-hardening phenomenon is mainly due to the extensibility limit of polymer chains. The first part of the GD model is equivalent to Hart-Smith model and then to the eight-chains (Arruda & Boyce 1993) and Gent models for the entire range of strains (Chagnon G. et al. 2004).

$$\frac{\partial W_1(I_1)}{\partial I_1} = h_1 e^{h_3(I_1-3)^2} \quad (4)$$

We proposed to remind the physical motivation of the second part of strain energy $W_2(I_2)$ of the GD model. As mentioned by (Treloar 1975), term that depends on I_2 in constitutive equations can be seen as corrections of the phantom network theory (I_1 function). We have proposed to constrain the eight-chains model by a new network of chains on the surface of the cube (figure 1). The confinement of the eight-chains model is governed by a strain energy potential. This potential constrains the eight-chains cube surface. Let us recall that the surface of the eight-chains model (a cube) is $I_2^{1/2}$ and that its increase under deformation is $I_2^{1/2} - 3^{1/2}$. We therefore define a pressure constrain of the eight-chains rubber network. This phenomenon is modeled by the second invariant energy part:

$$W_2(I_2) = 3h_2 \int \frac{1}{\sqrt{I_2}} dI_2 \text{ or } \frac{\partial W_2(I_2)}{\partial I_2} = \frac{3h_2}{\sqrt{I_2}} \quad (5)$$

where $3h_2$ stands for the pressure constrain of entanglement of the eight-chains rubber network.

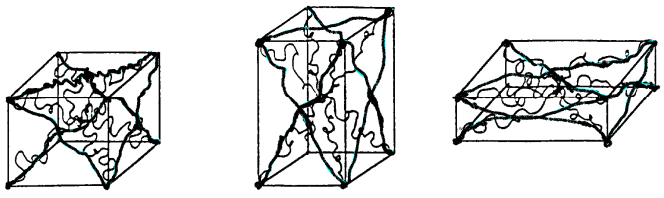

Figure 1. Entanglement of the eight-chains rubber network. Eight-chains model completed by surrounding chains (in bold) is the physical motivations of the GD model.

3 MULTIAXIAL EXPERIMENTAL DATA AND GD PARAMETERS IDENTIFICATION

In order to compare the efficiency of the models, we choose two complementary data sets issued from classical references (Marckmann & Verron 2006). The first set is due to Treloar (1944). In the current study, data from Treloar for unfilled natural rubber (cross-linked with 8 parts of S) were used. This material exhibits highly reversible elastic response and no stretch-induced crystallization up to 400%. Thus it is well-modeled by hyperelastic constitutive equations. Experimental measurements were performed for four different loading conditions: equibiaxial extension of a sheet (EQE), uniaxial tensile extension (UE), pure shear (PS) and biaxial extension (BE). The second data set is due to Kawabata *et al.* (1981). It was obtained using an experimental apparatus for general biaxial extension testing. In terms of stretch ratios, unfilled polyisoprene specimens were stretched from 1.04 to 3.7 in the first direction (λ_1) and from 0.52 to 3.1 in the perpendicular direction (λ_2). These values correspond to moderate strain but lead to deformation conditions from uniaxial extension to equibiaxial extension. Here, both experimental data sets are simultaneously considered to compare the models because the two materials are quite similar. Thus, for a given model, a unique set of material parameters must be able to reproduce these data with a good agreement. The parameter identification is performed using genetic algorithms as presented in (Marckmann 2004). The GD model assumes entanglement of the eight-chains rubber network and identified responses are depicted on figures 2-4. The GD model responses on figures 2 to 4 are almost equivalent to Ogden six parameters (Ogden 1972) results.

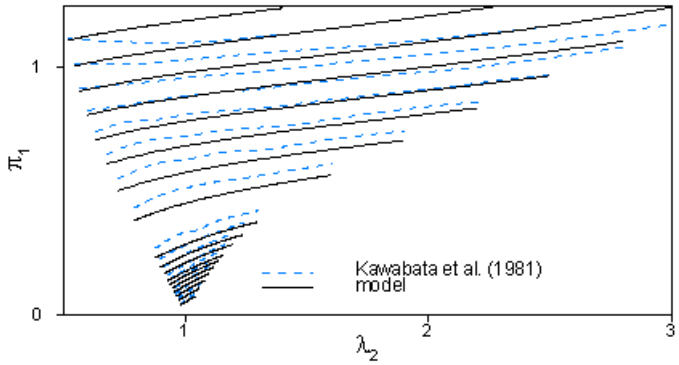

Figure 2. Experimental data (- -) and GD model identification for biaxial tensile tests. Piola-Kirchhoff function of extension for several transverse extensions. Incompressible GD model response.

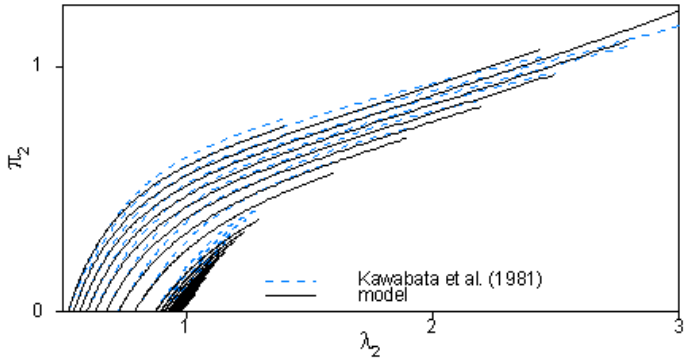

Figure 3. Experimental data (- -) and GD model identification for biaxial tensile tests. Piola-Kirchhoff function of extension for several transverse extensions. Incompressible GD model response.

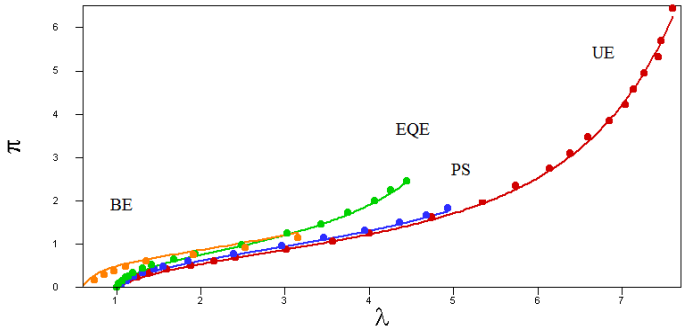

Figure 4. Experimental data (•) and GD model identification for biaxial extension (BE), equibiaxial extension (EQE), pure shear (PS), uniaxial tensile extension (UE). Incompressible GD model response.

The GD parameters are: h_1=0.142 MPa, h_2=1.585 10^{-2} MPa and h_3=3.495 10^{-4}. The proposed GD model is able to accurately reproduce the whole "S" shaped response of the material. The model behaves satisfactory under all the presented loadings (figures 2-4).

4 A UNIFIED DAMAGE MODEL FOR MULLINS AND FATIGUE MODELLING

4.1 *Material*

The material studied here is a carbon black-filled natural rubber. Its recipe and mechanical characteristics are given in Table 1. Samples are obtained by injection molding in order to reproduce industrial conditions of mass produced parts. The compound has been cured for 7 min, with a mold temperature set to 165°C. All samples were made using the same material batch to limit properties scattering due for example to mixing.

Table 1: Recipe and mechanical characteristics of the material

Formulation	
NR	100.00
Zinc Oxide	9.85
Plastificant	3.00
Carbon black	43.0
Stearic acid	3.00
Antioxidant	2.00
Accelerators	4.00
Mechanical characteristics	
Density	1.13
Shore hardness A	58
Failure stress (MPa)	22.9
Failure stretch (%)	635

4.2 *Damage modeling*

Elastomers present a loss of stiffness after the first loading cycle of a fatigue experiment (Mullins, 1969). It has been observed that this phenomenon is only dependent on the maximum deformation previously reached in the loading history of the material. It is quite important to model it because the mechanical behaviour of rubber products is highly modified by this softening phenomenon. The stress-softening for fatigue loadings should be explicitly included in the model. The continuum damage mechanics has often been used to model the Mullins effect even if phenomenon undergoing Mullins effect is not a strictly speaking an irreversible damage phenomenon. For example, it can be recovered with time and annealing accelerates this recovery. The general theory of Continuum Damage Mechanics is detailed in Lemaitre and Chaboche (1990) book. When applied to GD hyperelastic density, it yields to GDM model. This new strain energy function for hyperelastic model with damage variables can be written (eq 6) :

$$W_{GDM}(I_1,I_2)=\tilde{h}_1\int e^{\tilde{h}_3(I_1-3)^2}dI_1+3\tilde{h}_2\int\frac{1}{\sqrt{I_2}}dI_2 \qquad (6)$$

$$\tilde{h}_1=h_1(1-d_1),\ \tilde{h}_2=h_2(1-d_2),\ \tilde{h}_3=h_3(1-d_3)$$

The incompressible state laws (eq. 2) associated with this model are classically obtained by equation 7.

$$\sigma=\left.\frac{\partial W_{GDM}}{\partial B}\right|_{I_1=1} \qquad (7)$$

We define the thermodynamic forces Y_{d_i} associated to damage internal variables d_{iM} by:

$$-Y_{d_i}=\frac{\partial W_{GDM}}{\partial d_{iM}} \qquad (8)$$

The failure of rubber part under fatigue loadings is taken into account by three damage variables d_{1F}, d_{2F} and d_{3F}. The micro damage crack growth under high cycle fatigue can be considered as a combination of damages due to the Mullins Effect and due to the cyclic variation of the loading, hence total dam-

age evolution for three different material constants $\tilde{h}_i$ can be expressed as follows:

$$\dot{d}_i = \dot{d}_{iM} + \dot{d}_{iF} \qquad i = 1,2,3 \tag{9}$$

Where the term $\dot{d}_{iM}$ corresponds to Mullins Effect under few cyclic static loading and $\dot{d}_{iF}$ is related to high cyclic fatigue one. Variables $\dot{d}_i$ represent the total damage rate for each mechanical constant. The details of Mullins and fatigue damage variables will be discussed hereafter.

4.3 *Mullins effect damage evolution law*

For the Mullins part, a non-standard damage model is built here, the damage thermodynamics forces are not used to describe damage evolution laws. Instead of that, we consider that the quantity governing the damage evolution laws is the maximum value of the first invariant. This assumption is achieved according to the physical motivations of maximum strain state endured during the history of the deformation (Marckmann et al. 2002). In order to do this we can introduce damage criterion functions

$$f_i = I_1 - k_i(d_{iM}) \tag{10}$$

such as $f_i<0$ implies no damage evolution and as damage evolves at $f_i=0$ with then $d_{iM} = k_i^{-1}(I_1)$. Choosing particular expressions for k_i-functions allows to derive the damage evolution laws (equations 8-13) and makes the model complete for Mullins effect. This model is able to represent unloading Mullins effect responses (figure 12). Evolution equations of the damage variables are expressed thanks to the first strain invariant.

$$d_{1M} = d_{1\infty}\left(1 - \exp\left(-\frac{\underline{I}_1^{\max}}{\eta_1}\right)\right)$$
$$d_{2M} = d_{2\infty}\left(1 - \exp\left(-\frac{\underline{I}_1^{\max}}{\eta_2}\right)\right) \tag{11}$$

where $d_{1\infty}, \eta_1, d_{2\infty}, \eta_2$ and b are material parameters. $\underline{I}_1^{max}$ (or $\underline{I}_1$ in the following) represents the maximum value of the first strain invariant obtained during loadings. The coupling with damages d_{1M} and d_{2M} is similar to the discontinuous damage part of the constitutive equations proposed by Miehe (1995). Let us consider the mass conservation of the polymer network, which implies that the number of monomer segments per unit volume must remain constant (Marckmann et al. 2002). For the 8 chains model this assumption leads to: $C_R N = cst$. This equation is derived for the GDM model. Chagnon et al. 2004, suggest a relationship between parameters of the 8 chains model, HartSmith model and the Gent model. These relations lead to equation:

$$C_R N = 2h_1\left(\frac{J_m}{3} + 1\right) \tag{12}$$

Where the maximum value of $I_1 - 3$ is J_m in the Gent models.

According to relationship between parameters this leads to link the mechanical properties $\tilde{h}_1$ and $\tilde{h}_3$ and shows that d_3 is not an independent thermodynamics damage variables.

$$d_{3M} = 1 - F\left(d_{1M}\right),\ F\left(d_{1M}\right) = \frac{b}{h_3\left(3\left(a/\tilde{h}_1 - 1\right)\right)^2} \tag{13}$$

4.4 *High cycle fatigue damage evolution law*

The proposed high cycle fatigue part of the damage model is based on an improved method already proposed in (Gornet & Ijaz 2011) for composite materials. Hence, in case of fatigue loadings, we assume that the damage variables of the rubber part will be also governed by the maximum value of the first invariant during the cyclic loadings. In this article, a fatigue model based on damage maximum value of the first invariant release rates is proposed as follows:

$$\dot{d}_{iF} = \frac{\partial d_{iF}}{\partial t} = \begin{cases} g_i\left(d_i, \dfrac{\dot{\underline{I}}_1}{I_{1C}}, R = \dfrac{\underline{I}_{1\min}}{\underline{I}_1}\right)\dfrac{\dot{\underline{I}}_1(t)}{I_{1C}} \\ \text{if } \dot{\underline{I}}_1 \geq 0 \quad \text{and} \quad f_F \geq 0 \\ 0 \\ \text{if } \dot{\underline{I}}_1 < 0 \quad \text{or} \quad f_F < 0 \end{cases} \tag{14}$$

Where, f_F is a damage loading function and defines the threshold of fatigue damages growth. This function can be written in terms of the first strain invariant as $f_F = \underline{I}_1 - I_1^*$, where I_1^* is the first invariant threshold value and damage will grow only and only if $f_F \geq 0$. This threshold value I_1^* is assumed zero in this paper.

Here, g_i is a dimensionless function and depends on maximum value of the first invariant on the cycle $\underline{I}_1$. Since the damage growth defined by Equation (14) is in rate format, it should be integrated over each time increment in the numerical analysis in or-

der to obtain the damage at the end of increment. The damage variable at the end of a time increment Δt can be written as:

$$d_{iF}(N+\Delta N) = d_{iF}(N) + \int_N^{N+\Delta N} \dot{d}_{iF}\, dt = d_{iF}(N) + \frac{\partial d_{iF}}{\partial N}$$

$$d_{iF}(t+\Delta t) = d_{iF}(t) + \int_t^{t+\Delta t} \dot{d}_{iF}\, dt = d_{iF}(t) + \sum_{n=N}^{N+\Delta N} \mathrm{P}(d_i, \underline{I_1}) \tag{15}$$

Here t and $t+\Delta t$ are the times corresponding to end of cycles N and $N+\Delta N$ respectively. Here $\mathrm{P}(d_i, \underline{I_1})$ represents the small variation of damage within one cycle compared to total number of cycles and is expressed through following form:

$$\mathrm{P}(d_i, \underline{I_1}) = \frac{\partial d_{iF}}{\partial N} = \frac{\alpha_2(\underline{I_1})}{\alpha_1(\underline{I_1})\alpha_3(\underline{I_1})} \left(\frac{d_i}{\alpha_2(\underline{I_1})} \right)^{1-\alpha_3(\underline{I_1})} \exp\left(\frac{d_i}{\alpha_2(\underline{I_1})} \right)^{\alpha_3(\underline{I_1})} \tag{16}$$

Where α_i are three functions of the maximum value of the first strain invariant $\underline{I_1}$ obtained during the cyclic loading.

$$\alpha_1(\underline{I_1}) = \exp\left(a_1 + b_1 \log(\underline{I_1} - 3)\right)$$
$$\alpha_2(\underline{I_1}) = a_2 + b_2(\underline{I_1} - 3)$$
$$\alpha_3(\underline{I_1}) = a_3 + b_3(\underline{I_1} - 3) \tag{17}$$

The effect of load ratio "R", for loads varying between maximum and minimum values of I_1 during a cycle is not taken into account in the present study. The sum over the cycle numbers in Equation (15) can be approximated by using numerical integration schemes like trapezoidal rule or Simpson's rule for definite integrals. In the present paper we assume that fatigue damage evolution rate is equivalent for each variable d_{1F} and d_{2F} .

$$\dot{d}_F = \dot{d}_{1F} = \dot{d}_{2F} \tag{18}$$

According to relationship between parameters this leads to link the mechanical properties $\tilde{h}_1$ and $\tilde{h}_3$ and shows that for the unified Mullins and fatigue d_3 is not an independent thermodynamics damage variable.

$$d_3 = 1 - F_F(d_1),$$

$$F_F(d_1) = \frac{b_F}{h_3\left(3\left(a_F(N)/\tilde{h}_1 - 1\right)\right)^2} \tag{19}$$

$$a_F(N) = a_F e^{-\gamma N}$$

The last relationship suggests here that the number of structural monomers in the chain network can decrease during cyclic fatigue loading with the increase of dangling chains. Indeed, the mass conservation written in term of monomer in the rubber matrix (Eq. 12) must not be taken strictly. Damage can injure the chain structural network.

In order to verify the possibilities of the proposed fatigue damage evolution law. The global fatigue response of the cylindrical samples under cyclic uniaxial loadings (equations 20-21) are depicted on Figures 5-7 for several values of $\alpha_i(\underline{I_1})$ with $\lambda = 6.15, \underline{I_1} = 38.76$.

$$I_1 = \lambda^2 + \frac{2}{\lambda},\ I_2 = \frac{1}{\lambda^2} + 2\lambda,\ I_3 = 1 \tag{20}$$

$$\pi = \frac{F}{S_0} = 2\left(\lambda - \frac{1}{\lambda^2}\right)\left(\frac{\partial W}{\partial I_1} + \frac{1}{\lambda}\frac{\partial W}{\partial I_2}\right) \tag{21}$$

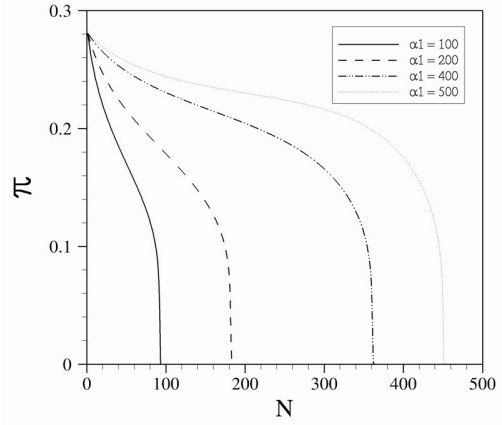

Figure 5. Variation of the adimensional Piola-Kirchhoff tensile stress with respect to ultimate Failure Cycles over the wide range of α_1 for $\lambda = 6.15, \underline{I_1} = 38.76$ with $\alpha_2 = 0.6$ and $\alpha_3 = 6$.

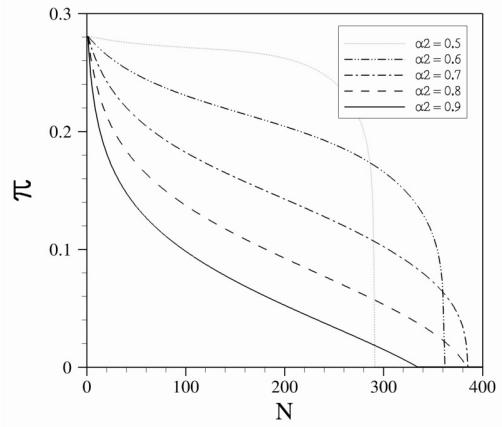

Figure 6. Variation of the adimensional Piola-Kirchhoff tensile stress with respect to ultimate Failure Cycles over the wide

range of α_2 , for $\lambda = 6.15, \underline{I}_1 = 38.76$ with $\alpha_1 = 400$ and $\alpha_3 = 6$.

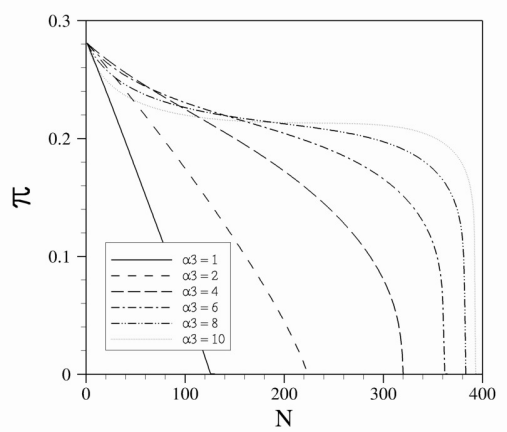

Figure 7. Variation of the adimensional Piola-Kirchhoff tensile stress with respect to ultimate Failure Cycles over the wide range of α_3 for $\lambda = 6.15, \underline{I}_1 = 38.76$. with $\alpha_1 = 400$ and $\alpha_2 = 0.6$.

5 EXPERIMENTAL CONTEXT

5.1 *Apparatus*

Linear actuators are used for experiments. The Linear actuator is servo-jack which maximum loading displacements is 100 mm, and maximum loading speeds is 0.6 m.s^{-1}. The maximum loading force is 3 kN. Fatigue tests are performed in a thermal oven, and the sample skin temperature is set to 23°C. It is possible to realize uniaxial combined tensile-compressive-torsion loadings with this equipment (Figure 8).

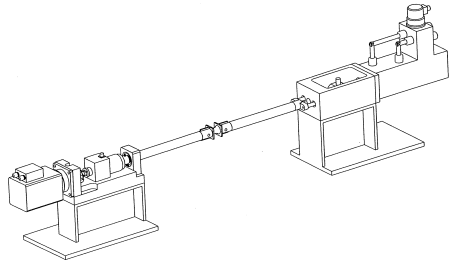

Figure 8. Tensile-torsion fatigue experiments (climatic chamber is not shown).

5.2 *Sample*

A classical test sample was used for this experimental and simulation campaign. The sample is called AE2 and the mesh is presented in Figure 9 (half of the specimen). It is an axisymmetric notched sample, the radius of the notch being equal to 2 mm. It is used in the case of uniaxial and multiaxial loading conditions, because its geometry induces a multiaxial stress state in the notch, even under uniaxial loading conditions.

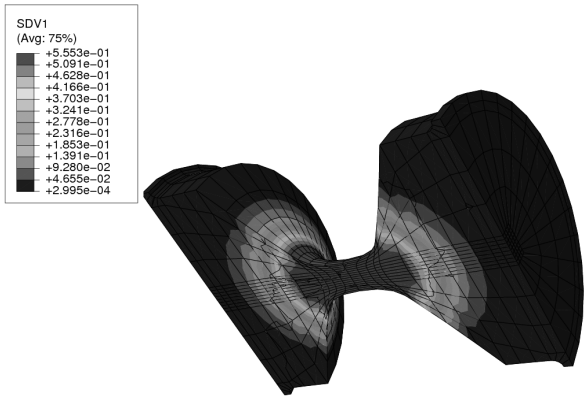

Figure 9. AE2 sample for static and fatigue loading. The maximum value of d_{1M} (Mullins effect) is in the center of the sample.

5.3 *Monitoring and data acquisition*

Both displacement (resp. angle) and force (resp. torque) can be monitored during fatigue test. A test is a series of cycle sequences. In this way, a large variety of tests can be conducted. Experimental data are recorded, such as the minimum and maximum displacements and forces, and the shape of hysteresis cycles. In this paper, the fatigue damage model is identified on idealized fatigue experimental data (Figure 10). The loading is an imposed axial displacement with constant sine amplitude. As example, the damage accumulation in AE2 specimen under tensile fatigue loadings is presented Figure 9. Experimental evolution of the hysteresis loop and GDM predictions obtained for non-relaxing uniaxial tensile experiments are presented on Figure 11.

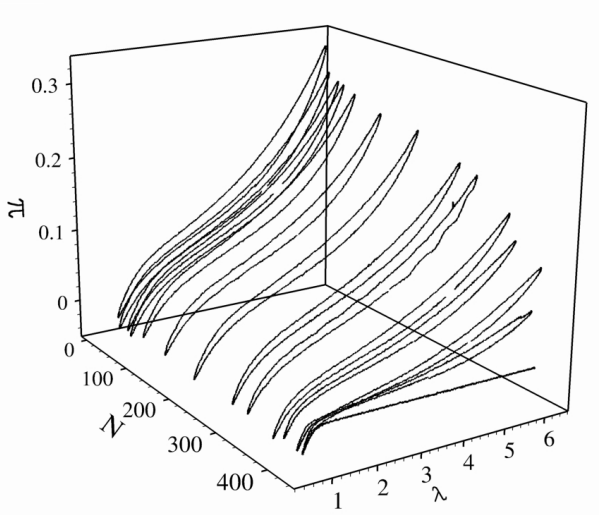

Figure 10. Experimental evolution of the hysteresis loop for an enforced displacement relaxing experiment on a AE2 sample. N represents the number of fatigue cycles.

In order to overcome identification problems of the parameters overs the 985 experimental cyclic responses an equivalent cylindrical sample is used to evaluate the local material response in the notch of the specimen. Piola-Kirchhoff stress responses are

then normalized. The offset of the cyclic loading, generally attributed to anisotropic and viscous effects, is also vanished since the present model cannot reproduce it.

5.4 *Identification of the parameters*

It must be highlighted that uniqueness of the parameters values is one of the fundamental underlying questions in inverse analysis. Genetic algorithms are used to explore the influence of parameters on the behavior responses. Figure 11 represents the tensile response of the damage model corresponding to experimental condition of Figure 10. This figure shows how the model is able to accurately reproduce the response of fatigue loadings for a maximal stretch.

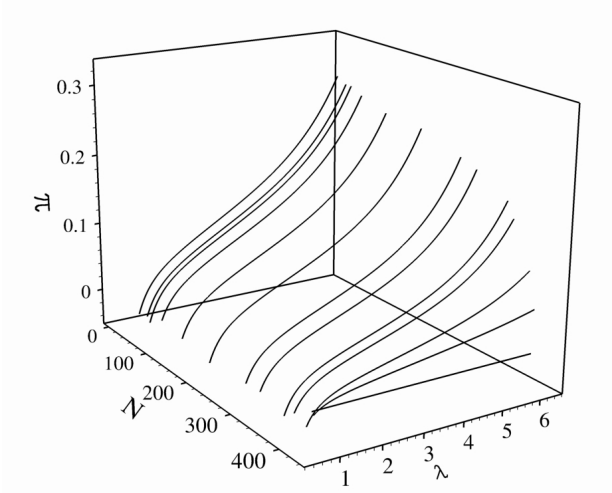

Figure 11. Simulations of the evolution of the averaging response of the hysteresis loop during fatigue loadings (AE2 under relaxing experiments. N represents the number of fatigue cycles.

Figure 12 represents the response of the identified model for fatigue cyclic extension to λ=10 and for several cycles. Even if the model cannot reproduce the hysteresis response of the material, the global pseudo-hyperelastic response can be accurately reproduced. The envelope of the maximum value of the stress for different extension are given in Figure 13 as function of the number of fatigue cycles for different values of extension. The corresponding curves directly derived from of Eq (20) and (21). The Mullins and cyclic fatigue effect of the damage model are presented (Figure 14). The above results showed the efficiency of our damage model to capture the rubber response under constant amplitude loading conditions. However, the model can also be used with variable amplitude cyclic loadings. The identified parameters for GDMF are given below:
h_1=0.02457 MPa, h_2=1.49 10^{-6} MPa and h_3=1.1883 10^{-11}, a_1=14.01, b_1=-1.564, a_2=0.61209, b_2=0.07659, a_3=7.3392, b_3=-0.05347,a_F=2.83, $\gamma = 0.0001146$, $d_{1\infty} = d_{2\infty} = .6896$, $\eta_1^{-1} = \eta_2^{-1} = 0.017269$

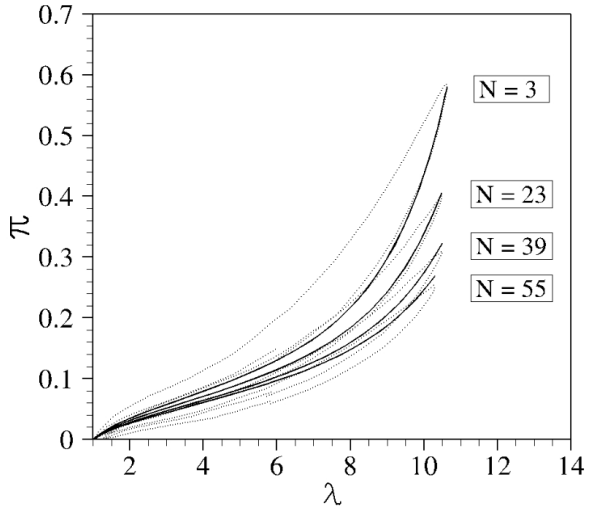

Figure 12. Fitted damage model response superimposed to experimental data for a AE2 sample. N in the legend stands for the number of fatigue cycles.

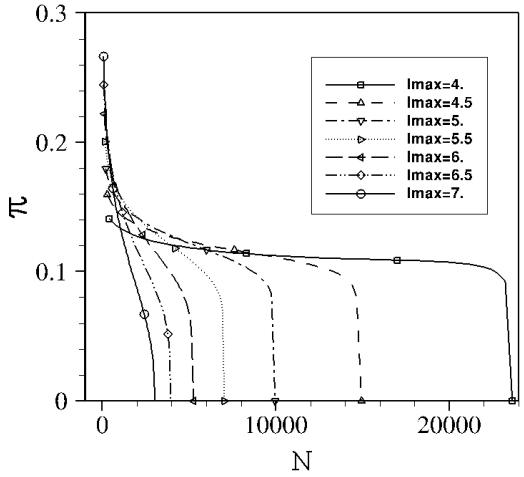

Figure 13. Piola-Kirchhoff functions of number of fatigue cycles (N) for several values of the maximum first invariant values of λmax.

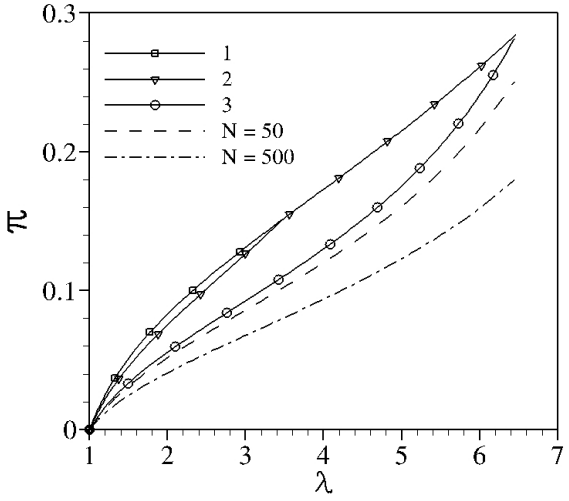

Figure 14. Model responses for tensile tests : load 1, 2 and 3 respectively from λ=1 to 3.5 (first time), 3.5 (second time) then 6.5 (first time) and 6.5 (second time). Fatigue effect of the response for cycle 50 and 500.

6 CONCLUSIONS

We propose here a simple isotropic hyperelastic model (GD) expressed in terms of classical independent strain invariants of the symmetric Cauchy-Green tensor. The strain-energy part as function of I_1 is to the same as the one of the Hart-Smith model. Moreover, this part is equivalent to the Eight chain model. Concerning the function of the second invariant I_2 a square root part is proposed. The corresponding energy density contribution is connected to the non-affine deformation of the entanglement Eight-chains network. The Mullins and fatigue effects are then modeled through 3 damage variables. The model is thus derived stating that the loss of stiffness depends on the maximum value of the first invariant I_1 under Mullins and fatigue loadings. An inverse optimization technique is used in order to adjust the fatigue damage parameters on tensile fatigue tests. The constitutive equations were presented in their most general form and can be adapted to all hyperelastic rubber form. The propose model can describe successfully the experimental response for low and high cyclic uniaxial extensions. The performance of the proposed model is presented for the fatigue life response of AE2 rubber samples under tensile fatigue loadings. The model provides a good agreement between experimental stiffness decrease and the numerically AE2 adjusted one.

7 REFERENCES

Arruda E. & Boyce M.C. 1993. A three dimensional constitutive model for the large stretch behavior of rubber elastic materials. *J. Mech. Phys. Solids*, 41, 2, 389-412

Ayoub, G. Naït-Abdelaziz, Zaïr F. Gloaguen, J.M., Charrier, P. 2012. *Mechanics of Material*, 52, 87-102.

Cantournet, S. 2202. Endommagements et fatigue des élastomères, Thèse de l'Université Pierre et Marie Curie.

Cantournet, S. Desmorat, R. Besson J. 2009. Mullins effect and cyclic stress softening of filled elastomer by internal sliding and friction thermodynamics model. *International Journal of Solids and Structures*, 2256-2264.

Chagnon G. Marckmann G. and Verron E. 2004. A comparison of the hart-smith model with arruda-boyce and gent formulations for rubber elasticity, *Rubber Chemistry and Technology*, 77, 724-735

Chagnon, G. Verron, E. Gornet, L. Marckmann, G. & Charrier, P. 2004. On the relevance of continuum damage mechanics as applied to the Mullins effect in elastomers. *J. Mech. Phys. Solids*, 52, 1627-1650.

Chagnon, G. Verron, E. Marckmann, G. Gornet, L. 2006. Development of new constitutive equations for the Mullins effect in rubber using the network alteration theory. *International journal of solids and structures* 43 (22-23), 6817-6831

Gornet, L. Marckmann, G. Desmorat R., Charrier P. 2012. A new isotropic hyperelastic strain energy function in terms of invariants and its derivation into a pseudo-elastic model for Mullins effect: application to finite element analysis, *Constitutive Models for Rubber VII,* pp. 265-271.

Gornet L., Ijaz H. High cycle fatigue damage model for delamination crack growth in CF/epoxy composite laminates, *Composite Part B*, 42, 1173-1180, 2011.

Hart-Smith, L. J. 1966. Elasticity parameters for finite deformations of rubber-like materials. *Z. angew. Math. Phys*. 17, 608-626

Kawabata, S., Matsuda, M., Tei, K., and Kawai, H. 1981, *Macromolecules* , 154–162.

Lambert-Diani J., Rey C., New phenomenological behavior laws for rubbers and thermoplastic elastomers, *Eur. J. Mech. A/Solids*, 18, 1027-1043, 1999.

Lemaitre, J. & Chaboche, J. L. 1990. *Mechanics of solid materials*, Cambridge University Press.

Marckmann G., E. Verron 2006. Comparison of hyperelastic models for rubberlike materials, *Rubber Chemistry and Technology*. 5, 835-858

Marckmann, G. 2004. Contribution à l'étude des elastomers et des membranes souflées, Thèse de Doctorat, Centrale Nantes.

Marckmann, E. Verron, L. Gornet, G. Chagnon, P. Charrier and P. Fort, A theory of network alteration for the Mullins effect, *J. Mech. Phys. Solids* **50** (2002), pp. 2011–2028

Miehe, C. 1995. Discontinuous and continuous damage evolution in Ogden type large strain elastic materials. *Eur. J. Mech., A/Solids* 14, 697-720.

Mullins, L. 1969. Softening of rubber by deformation. *Rubber Chem. Technol*. 42, 339-362.

Ogden, R. W., 1984. Recent advances in the phenomenological theory of rubber elasticity. Rubber Chemistry and Technology. 59, 361–383.

Ogden, R. W., 1972. Large deformation isotropic elasticity - on the correlation of theory and experiment for incompressible rubberlike solids. Proc. R. Soc. Lon. A. 326, 565–584.

Treloar, L. R. G. 1975, The Physics of Rubber Elasticity, Oxford Classic Texts.

Treloar, L. R. G. 1944, *Trans. Faraday Soc.* , 59–70.

Wang, B. Lu., H. Kim G.H. 2002. A damage model for fatigue life prediction under multiaxial loading. *Mech. Mater.*, 34,475-483.